Alumina Supported Iron Catalysts for the Selective Acetylene Hydrogenation under Industrial Front-End Conditions†

Hannah Lamers,[a] *Malte Schummer,*[a] *Martin Lucas,*[a] *Marcus Rose**[a]

[a] Technical University of Darmstadt, Ernst-Berl-Institute of Technical and Macromolecular Chemistry, Peter-Grünberg-Straße 8, 64287 Darmstadt, Germany

E-mail: marcus.rose@tu-darmstadt.de (MR)

† Electronic supplementary information (ESI) available. All data presented in this publication are available from the open access repository Repo4Cat (https://hdl.handle.net/21.11165/4cat/73bc-a64s).

ABSTRACT:

The removal of acetylene traces from ethylene streams coming from the steam cracker is carried out in the industry on an annual scale of several million tonnes using Pd-Ag/Al_2O_3 catalysts. The substitution of palladium containing catalysts with more abundant, cheap and non-toxic materials is a first crucial step towards a more sustainable chemical industry. Since iron is one of the most abundant metals and can be mined in almost all regions world wide, it is an ideal catalyst material. In this work, we present the development of alpha alumina supported iron catalysts with 1 wt%, 5 wt% and 10 wt% iron loading and their application in the selective acetylene hydrogenation under industrially applied front-end conditions. The catalysts were prepared via simple incipient wetness impregnation and were analyzed via XRD, XRF, TPR, TEM and N_2-Physisorption. The catalysts were subsequently calcined, reduced and tested in the selective acetylene hydrogenation. After an activation phase, the catalysts show excellent activity and selectivity in the acetylene hydrogenation at 90 °C without significant ethylene hydrogenation. The excellent catalytic activity underline the great potential of iron based catalysts as an alternative to conventional Pd-containing materials.

KEYWORDS: *Heterogenous Catalysis, Acetylene Hydrogenation, Front-End Conditions, Semihydrogenation, Supported Iron nanoparticles.*

1 Introduction

Ethylene is one of the most important platform chemicals due to its application as monomer in polymer production and as reactant for the production of intermediate products such as dichloroethane, ethylene oxide, ethyl benzene and vinyl acetate.[1,2] The conventional route for the production of ethylene is the cracking of naphta or recently, the production from bioethanol by dehydration. The cracking conditions mainly favour the formation of olefins as well as the formation of smaller amounts of multi unsaturated compounds.[1] High purity ethylene streams are required especially in polymer production to ensure reproducible product qualities. Multi-unsaturated impurities such as acetylene lead to poisoning of Ziegler-Natta catalysts in polymerization reactions.[3–5] Therefore, the generation of ethylene-rich streams with acetylene concentrations lower than 1 ppm are necessary.[3–7]

Industrially, two main operating methods are commonly used for acetylene removal, tail-end and front-end operation. In the first case, the acetylene removal unit is located after the de-ethanizer. The feed contains only C_2-fractions and stoichiometrically added hydrogen.[6–10] The low hydrogen concentration guarantees a high selectivity for conversion of acetylene to ethylene avoiding the overhydrogenation to ethane. However, it favors increased oligomer and green oil formation leading to shorter catalyst lifetimes in the acetylene hydrogenation. Due to the lower risk of reactor runaway, hydrogenation under tail-end conditions is most widely used in industry and well researched.[7,10–12] The hydrogenation under front-end conditions takes place in front of the demethanizer[8] and therefore, the feed contains high hydrogen concentration as well as carbon monoxide and methane.[3,4,6,10,12,13] This carries the risk of overhydrogenation and hot spot formation.[4] The key advantage of front-end conditions is the improved process integration

combined with longer catalyst life cycles and has been studied intensively in the recent years.[4,13-15]

State of the art catalysts for both operation modes are palladium based catalyst systems.[4,6,7,12] Owing to the low availability of palladium, its mining process consumes large amounts of fresh water[16] and has a low atom economy,[16,17] while producing high amounts of carbon dioxide[18,19] due to high electricity consumption.[16,17,19] It is therefore important to reduce or substitute the use of this critical raw material. In order to reduce the amount of palladium required and increase the selectivity of the acetylene hydrogenation reaction, palladium single-atom catalysts[20,21] and palladium single sites incorporated into bimetallic systems have been the focus of recent research in this field. Some examples of bimetallic materials are PdAg[22–26], PdAu,[22,25,27,28] PdIn,[29] PdGa[22,30,31] as well as PdCu[22,32] and PdZn[5,20,22,33] compounds and the incorporation of Pd into metal-organic frameworks (MOF).[34]

The substitution of palladium by more abundant metals as active species is even more favorable. Therefore, intermetallic phases and alloys of bi- and trimetallic palladium-free catalyst systems such as supported AuAg[35], AgNi[36] and NiIn[37] systems as well as Cu-Ni-Fe systems[38] have been tested and show high activity and selectivity in the acetylene hydrogenation. Studt et al. performed DTF calculations to identify non-precious metal alloys as catalysts for selective acetylene hydrogenation.[39] They predicted and confirmed the suitability of NiZn and $NiZn_3$ as well as FeZn alloys as catalysts with high selectivity and activity.[39]

A promising way to replace palladium as catalyst is the use of pure iron catalysts for the selective acetylene hydrogenation. Zero-valent iron as well as Fe^{II} and Fe^{III} are known for their hydrogenation activity.[40–45] Furthermore, iron is one of the most abundant metals resulting in a low carbon foodprint and low water consumption during its production.[17]

Tejeda-Serrano et al. published the application of a Fe^{III}-O metal-organic framework as catalyst for the acetylene hydrogenation under front-end conditions.[45] The iron-based MOF reduces the acetylene content from 1.2 % to less than 10 ppm at 150 °C while ethane formation remains below 10 %. The increase of ethane formation over time indicates degradation of the catalyst under reaction conditions.[45]

More recently, Hock et al. published zero-valent iron nanoparticles as a very promising catalyst under front-end conditions.[15] The catalyst shows good activity of 14 % acetylene conversion at 90 °C and excellent selectivity. In addition, the selectivity could be improved by adding carbon monoxide as selectivity directing agent.[15]

Based on these results, the systematic investigation and optimization of the catalytic properties of the above mentioned iron nanoparticles is of interest. Therefore, we developed supported iron nanoparticles with different iron loadings as catalysts for the selective acetylene hydrogenation under industrially relevant front-end conditions. This results in catalysts with smaller iron particle sizes, higher surface area and improved dispersion, leading to catalysts with excellent performance and selectivity.

2 Experimental

2.1 Materials

Hydrogen (H_2, N50), methane (CH_4, N25), ethylene (C_2H_4, N35), an acetylene/propane/methane-mixture (1.2 mol% C_2H_2, 1 mol% C_3H_8, N25, remaining CH_4, N25) and argon (Ar, N50) were purchased from Air Liquide. Iron(III) nitrate nonahydrate ($Fe(NO_3)_3 \cdot 9\ H_2O$, 99 %) was purchased from Acros Organics, aluminum oxide (α-Al_2O_3, 99.95 %) from thermo scientific and iron(III)oxide (Fe_2O_3, 96 %) from Sigma-Aldrich. All materials were used as purchased.

2.2 Synthesis of supported Iron Nanoparticles

The synthesis of supported iron nanoparticles was carried out via incipient wetness impregnation. Catalysts with iron loadings of 1 wt%, 5 wt%, and 10 wt% were synthesized. The respective quantities of iron nitrate nonahydrate were dissolved in the volume of water corresponding to that of the pores in the alpha-alumina support. The pore volume of aluminum oxide was determined through N_2 physisorption. Subsequently, the iron nitrate solution was added dropwise to the support, was mixed until a homogeneous paste was obtained and was treated in an ultrasonic bath for 30 minutes. The paste was dried over night in a vacuum oven at 60 °C. Due to the low pore volume and surface area of α-Al_2O_3, the impregnation resulted in inhomogeneous distribution of iron nitrate as a crust on the surface. Therefore, the impregnated catalyst was mortared in acetone till all liquid is evaporated to ensure that the Fe-species is homogeneously distributed. The dried impregnated catalyst was then calcined in air at 600 °C for four hours (ramp: 5 °C min^{-1}, 100 mL min^{-1} Air). Right before the catalytic testing, the catalyst was reduced in hydrogen at 900 °C for three hours (ramp: 10 °C min^{-1}, 100 mL min^{-1} H_2).

2.3 Catalyst Chraracterization

The catalysts were analyzed with X-ray diffraction, X-ray fluorescence, temperature-programmed reduction, N_2-physisorption and TEM. Detailed information regarding the measurement protocol of each method can be found in the supporting information.

2.4 Selective semi-hydrogenation of Acetylene

A continuously operated fixed-bed reactor is used for the catalytic testing of the iron-based catalysts. A filter frit with a pore size of 5 µm is inserted into the tubular reactor to position the powdered catalyst. Prior to the reaction, the reduced catalyst was removed from the reduction

furnace, exposed to air and 200 mg of catalyst was weighed into the tubular reactor. In each experiment the temperature was varied between 30 °C and 90 °C at 22.5 bar. The feed composition corresponds to that of an acetylene removal unit (ARU) under front-end conditions (Table 1). A scheme of the experimental setup is included in the supporting information (Figure S4).

Table 1: Feed composition and flow rate applied to all experiments.[4]

Flow	12.5 L h^{-1}
x(C_2H_2)	0.4 mol%
x(C_2H_4)	39 mol%
x(H_2)	25 mol%
x(C_3H_8)$_{standard}$	0.34 mol%
x(CH_4)	35.26 mol%

The feed composition was realized by adding the different gas mixtures listed in chapter 2.1 through mass flow controllers. The composition of the output was monitored via GC with a FID analyzer. Detailed Information regarding the GC Method and the column can be found in the supporting information (GC program, Table S1). In each experiment the temperature is varied from 30 to 90 °C in 10 °C steps. Every temperature step was held for 100 min.

3 Results and discussion

The synthesized supported iron nanoparticles were analyzed by XRD, XRF, N_2-physisorption, TEM and TPR measurements. The catalyst with 1 wt%, 5 wt% and 10 wt% iron loading were tested as catalysts in the acetylene hydrogenation under industrial relevant front-end conditions.

3.1 Synthesis and Characterization

The catalysts with 1 wt%, 5 wt% and 10 wt% iron loading supported on α-Al_2O_3 were synthesized by incipient wetness impregnation using water and acetone as solvents. The catalyst precursors were calcined at 600 °C. The iron loadings of the resulting iron oxides on α-Al_2O_3 were determined by X-ray fluorescence using a calibration (Figure S1). The actual values were close to the target values, indicating a successful synthesis (Figure S2). Immediately prior to catalytic testing, the solids were reduced in hydrogen atmosphere at 900 °C. The reduction temperature was determined by TPR. The reduction profile of the supported iron oxides with 1 wt%, 5 wt% and 10 wt% iron loading showed the reduction pathway from Fe_2O_3 to Fe^0 for different iron loadings. It is reported in the literature, that the reduction of supported Fe_2O_3 in hydrogen atmosphere follows a two-step reduction:[46]

$$3\ Fe_2O_3 + H_2 \rightarrow 2\ Fe_3O_4 + H_2O$$

$$Fe_3O_4 + H_2 \rightarrow 3\ Fe + 4\ H_2O$$

The TPR patterns (Figure 1) show two distinct peaks. The catalysts with higher iron loading of 5 wt% and 10 wt% show peaks at about 400 °C and between 630 and 700 °C. The first peak indicates the reduction of Fe_2O_3 to Fe_3O_4. Fe_3O_4 is further reduced to Fe^0 at the second peak. The peak intensities correlate with the hydrogen consumption for each reduction step and the iron loading. For supported catalysts, the interaction between the metal particles and the support at high temperatures is reported.[47] The peak shoulder at about 800 °C indicates the formation of iron aluminates. The peaks are shifted for the catalyst with 1 wt% iron loading. The reduction of Fe_2O_3 to Fe_3O_4 occurs at lower temperatures of around 300 °C while the reduction to Fe^0 is shifted to significantly higher temperatures between 800 °C and 1000 °C. In addition, a peak broadening occurs at high temperatures. The peak broadening and the high reduction temperature are related

161 to small particle sizes at lower loadings and stronger interactions between the Fe particles and the
162 support favoring the formation of iron aluminates. To ensure complete reduction of the iron
163 catalysts and to maintain the same reduction procedure in all three cases, the reduction temperature
164 was set to 900 °C.
165

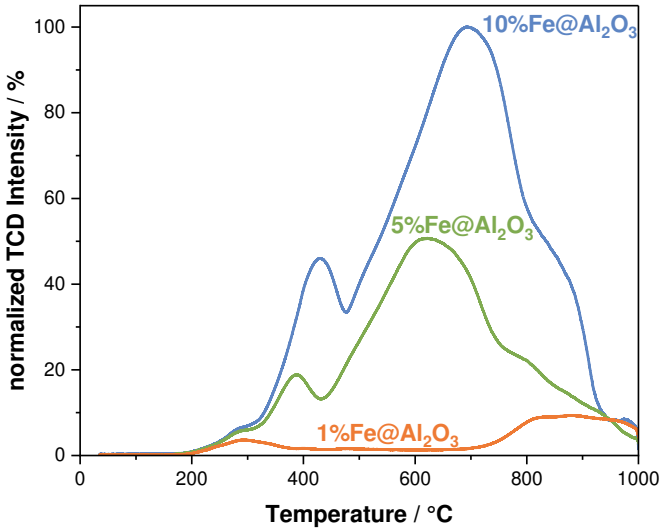

166

167 *Figure 1: TPR pattern of the catalysts with 1 wt%, 5 wt% and 10 wt% iron loading between 30 °C and 1000 °C.*

168

Figure 2 shows the diffraction pattern of the catalysts a) after calcination and b) after reduction. The calcined catalyst (a) shows α-Al_2O_3 reflexes (gray)[48] and Fe_2O_3 reflexes (red)[49] with lower intensity. The intensity of Fe_2O_3 reflexes increases with increasing Fe loading. No other iron oxide species were observed. After reduction at 900 °C all Fe_2O_3 reflexes disappear and the diffraction pattern of Fe^0 becomes visible (orange),[50,51] indicating complete reduction. The reflexes of Fe_2O_3, α-Al_2O_3 as well as Fe^0 are in good agreement with literature data.[50,51,48,49]

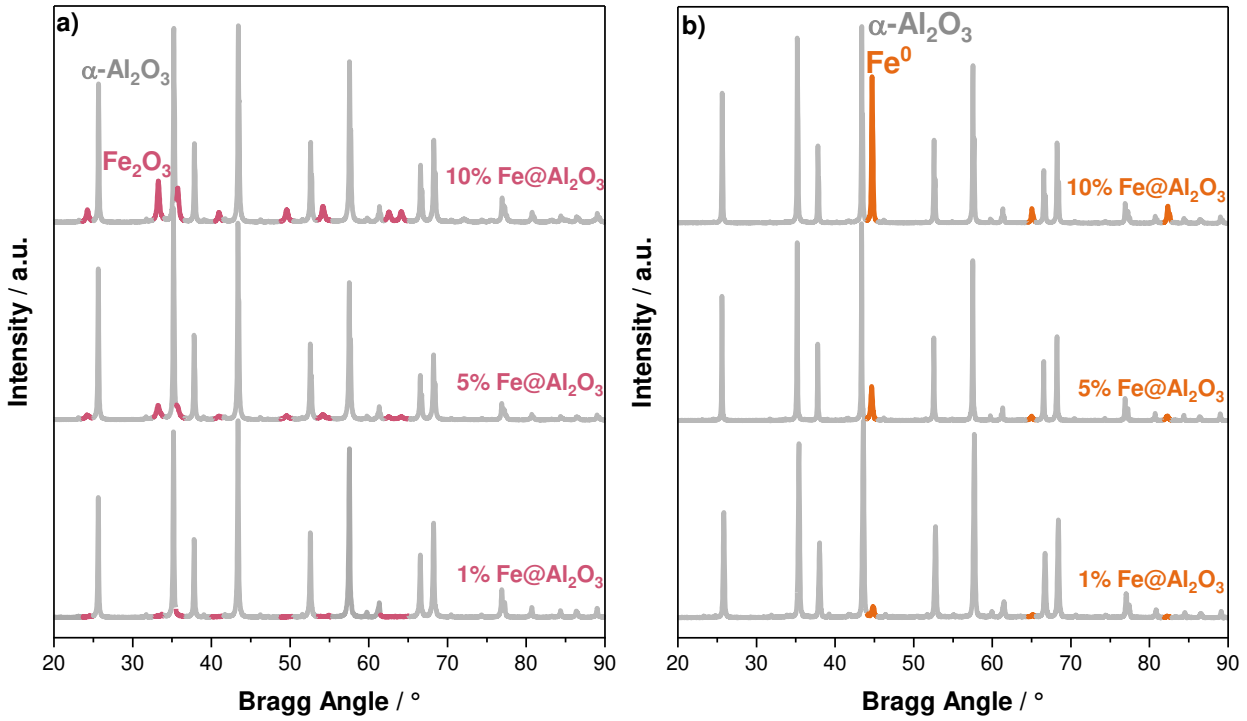

Figure 2: a) XRD measurements of the calcined catalysts with 1 wt%, 5 wt% and 10 wt% Fe-Loading. b) XRD measurements of the reduced catalysts with 1 wt%, 5 wt% and 10 wt% Fe-Loading.

The crystallite size of iron oxide and Fe^0 nanoparticles on alpha alumina support was determined using the Scherrer equation. To calculate the crystallite size of Fe_2O_3, the Scherrer equation was applied for the (211) reflexes at 23° 2θ, the (222) reflexes at 32.5° 2θ, the (510) reflexes at 48.5° 2θ and the (440) reflexes at 54.5° 2θ. The crystallite size of Fe^0 for the reduced iron catalysts was

184 determined analogously using the (110) reflexes at 44.5° 2θ, the (200) reflexes at 65° 2 θ and the
185 (211) reflexes at 82.5° 2θ. The average crystallite size of all reflections of Fe_2O_3 and Fe^0 for 1 wt%,
186 5 wt% and 10 wt% iron loading are shown in Table 2. The crystallite size of the reduced iron
187 particles increases increases in comparison to the Fe_2O_3 particles due to the high reduction
188 temperature of 900 °C indicating sintering. The crysalite sizes for the alpha alumina support is
189 added to the supporting information.
190
191 *Table 2: Crystallite sizes of the unreduced and reduced catalysts with 1 wt%, 5 wt% and 10 wt% iron loading.*

	Crystalite size (calc. cat.) / nm	Std. dev / nm	Cryststalite size (red. cat.) / nm	Std. dev / nm
1 wt% Fe@Al_2O_3	-	-	26.6	0
5 wt% Fe@Al_2O_3	20.0	1.4	31.2	2.4
10 wt% Fe@Al_2O_3	25.2	1.2	48.7	4.2

192
193 Transmission electron microscopy was used to identify the iron dispersion and the size of the
194 reduced iron nanoparticles (Figure 3).

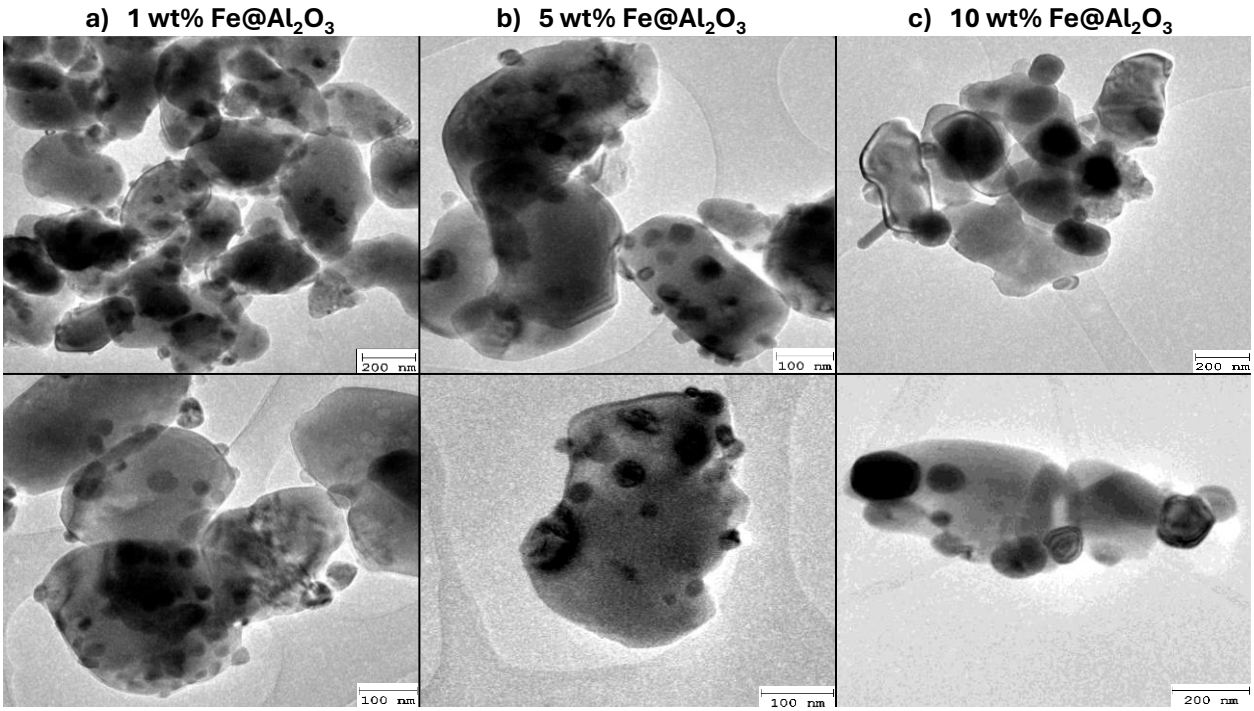

Figure 3: TEM images of the reduced catalysts with a) 1 wt% iron loading, b) 5 wt% iron loading and c) 10 wt% iron loading.

The TEM images show that the iron nanoparticles (darker spots) are deposited on the surface of the α-alumina support (brighter particles). As the loading increases, the size of the nanoparticles increases. Lower iron loadings lead to higher interaction between the support and the iron as well as to a higher dispersion.

N_2-physisorption measurements of the unreduced catalysts show that the impregnation of iron has no significant effect on the specific surface area compared to pure aluminum oxide (Figure S3).

3.2 Acetylene Hydrogenation

Catalytic tests of the above mentioned catalysts with 1 wt%, 5 wt% and 10 wt% Fe loading were carried out in a fixed bed reactor at temperatures between 30 °C and 90 °C and a pressure of 22.5 bar aiming to model industrial front-end conditions of an acetylene removal unit.[4] The feed

composition is given in Table 1. The observed product spectrum and the reaction pathways are shown below (Scheme 1). In general, catalysts with low selectivity towards ethane and the oligomerization products are suitable for the acetylene hydrogenation.

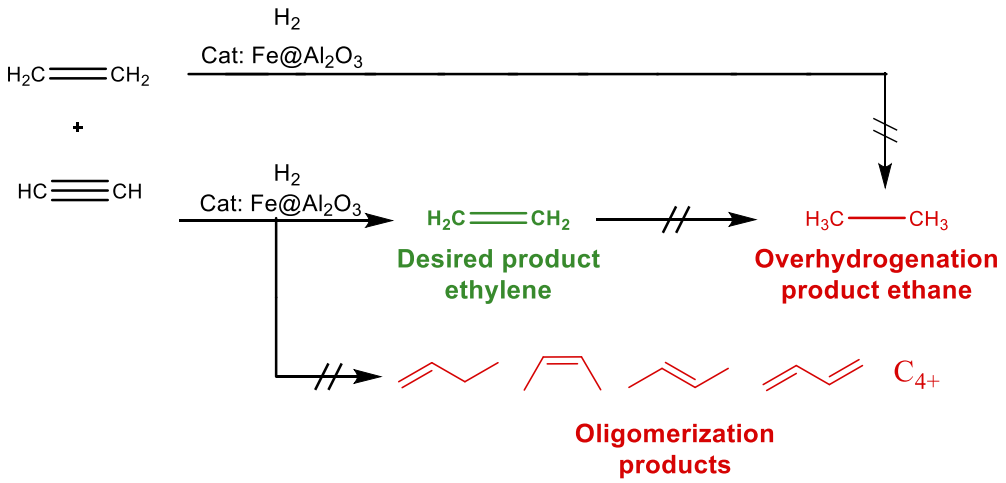

Scheme 1: Reaction scheme for the acetylene hydrogenation under front-end conditions including the desired product ethylene, the undesired overhydrogenation product ethane and the oligomerization products Z-butene, E-butene, 1-butene, butadiene, and higher oligomerization products C_{4+}.

Prior to the catalytic testing in the acetylene hydrogenation, the catalysts were reduced at 900 °C and transferred to the reactor as quickly as possible. At 90 °C under constant reaction conditions, the activation of each catalyst was observed at the beginning of the catalytic test (Figure 4, left). The activity shows a steep increase and reaches a plateau after 40 h time on stream. Afterwards, the temperature was varied between 30 °C and 90 °C in 10 °C steps, with stable activity and selectivity for each temperature (Figure 4, right).

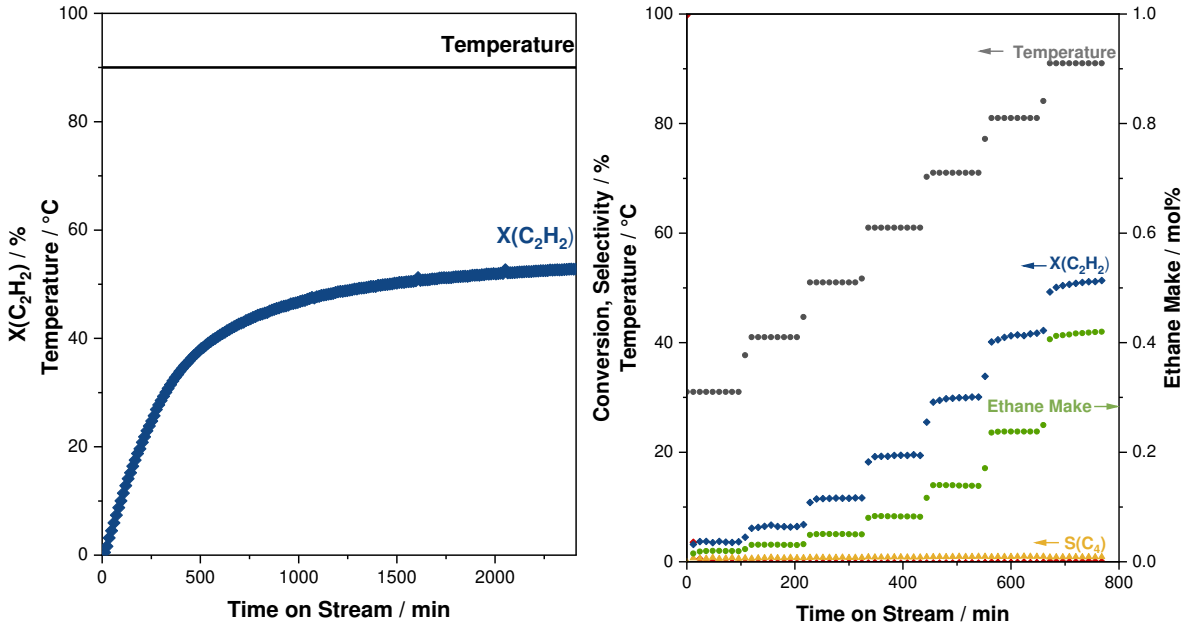

Figure 4: Left: Activation behavior, conversion of acetylene under reaction conditions at 90 °C exemplarily shown for the catalyst with 5 wt% iron loading in the first 40 h time on stream. Right: Acetylene (blue) and ethylene (red) conversion as well as C4-selectivity (yellow) and ethane make (green) for the 5 wt%Fe@Al_2O_3 catalyst after the activation phase.

The increase in activity with time at constant temperature and feed composition might indicate the reduction of remaining oxidic species on the surface and the formation of the active species under reaction conditions. The oxidic species originates from contact with air as the reduced catalyst is transfered from the reduction furnace to the reactor. The reducing reaction conditions seem to be able to reduce the catalyst surface in situ at 90 °C. Therefore, the synthesized catalysts with 1 wt%, 5 wt% and 10 wt% iron loading were tested in the acetylene hydrogenation following the same reaction protocol:

1) Catalyst treated at 90 °C for 40 h under reaction conditions (Table 1)
2) Cooling to 40 °C in methane atmosphere
3) Heating under reaction conditions in 10 °C steps from 40 to 90 °C with a heating ramp of 1 °C per minute and detection of the conversions and selectivities via GC

The acetylene conversion and the ethane selectivity of the different catalysts after the activation phase between 30 °C and 90 °C are shown in Figure 5.

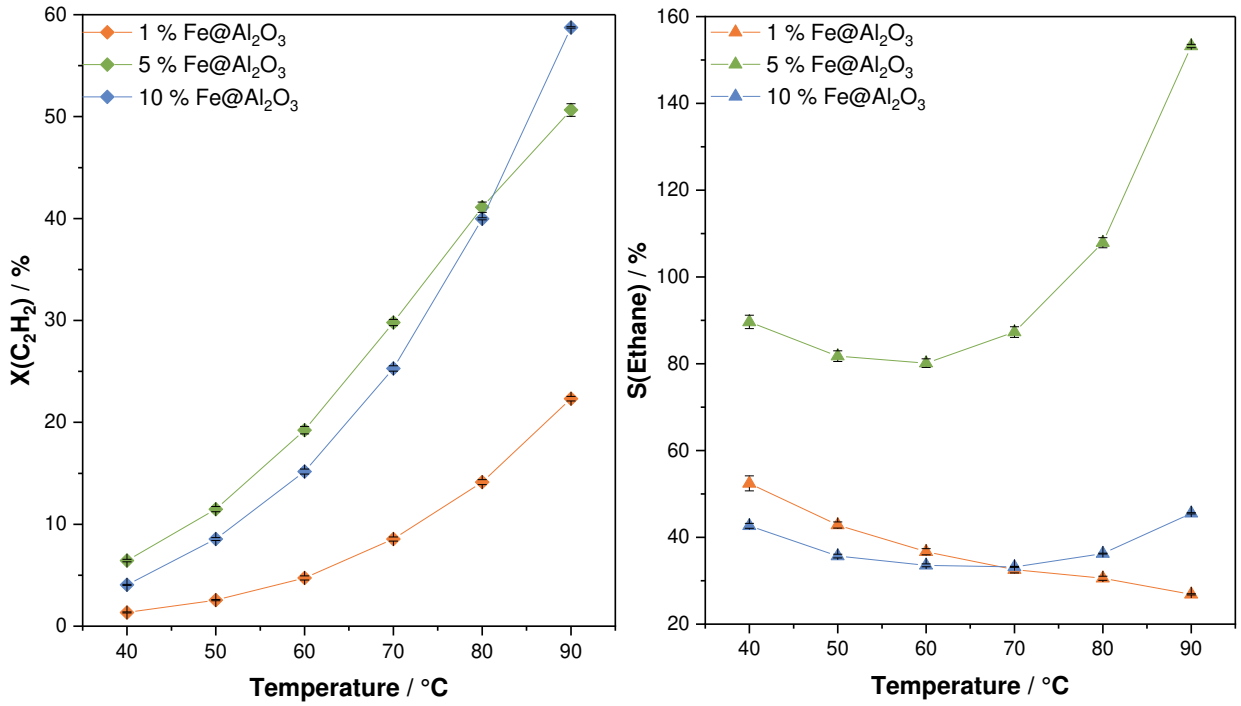

Figure 5: Left: Acetylene conversions between 30 °C and 90 °C for the catalysts with 1 wt% (orange), 5 wt% (green) and 10 wt% (blue) iron loading. Right: Ethane make between 30 °C and 90 °C for the catalysts with 1 wt% (orange), 5 wt% (green) and 10 wt% (blue) iron loading.

The acetylene conversion of the catalysts (Figure 5, left) with 1 wt%, 5 wt% and 10 wt% iron loading increases with increasing temperature, while the activity of the catalyst with 5 wt% and 10 wt% iron loading shows the highest activity. The catalyst with 5 wt% iron loading shows the highes activity at lower temperatures. The activity of the catalyst with 10 wt% iron loading exceeds its activity only at 90 °C. When looking at the selectivity to ethane (Figure 5, right), values above 100 % were obtained. This is due to the fact that the ethane selectivity was calculated based on the acetylene conversion. Since ethane can also be formed by hydrogenation of ethylene, ethane selectivities above 100 % are possible, but not desirable. The selectivity to ethane shows a similar

behavior for the catalyst with 5 wt% and 10 wt% iron loading, with a minimum of selectivity to ethane at around 60 °C and higher selectivity to ethane at higher and lower temperatures. The catalyst with 5 wt% iron loading shows the highest overall selectivity to ethane. It is noticeable, that the selectivity of the catalyst with 1 wt% iron loading decreases with increasing temperature. Therefore, the selectivity seems to be related to iron loading and particle size respectively, indicating that low iron loadings lead to excellent selectivitys of the catalyst. To evaluate the activity of the catalysts per gram of active component, the reaction rate for the hydrogenation of acetylene is determined.

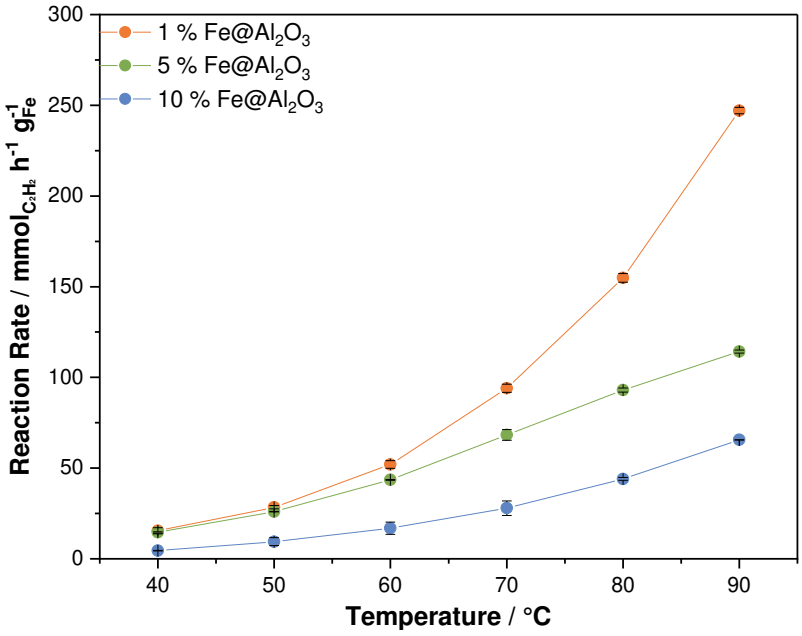

Figure 6: Reaction rate of the acetylene hydrogenation normalized by the mass of iron..

The calculation of the reaction rates show that the catalyst with 1 wt% iron loading has the highest overall values, followed by the catalysts with 5 wt% and 10 wt% iron loading. While the catalysts with 5 wt% and 10 wt% iron loading show an approximate linear increase of the reaction rate, the

catalyst with 1 wt% iron loading shows an approximate exponential progression. Therefore, the catalyst with an iron loading of 1 wt% exceeds the reaction rates of catalysts with 5 wt% and 10 wt% iron loading. The results underline the high catalytic activity of iron catalysts with lower iron loading.

The results of the catalytic tests of iron-based catalysts with iron loadings of 1 wt%, 5 wt% and 10 wt% show excellent activity and selectivity in the acetylene hydrogenation under industrial front-end conditions, especially for the catalyst with the lowest iron loading. Furthermore, the catalytic activity exceeds that of unsupported iron nanoparticles, clearly demonstrating the improved properties of the supported catalysts.

4 Conclusion

The goal of this work was to improve the catalysts' properties and the catalytic activity of monometallic iron catalysts by supporting on alpha alumina and to underline the great suitability of iron as catalyst in industrial relevant applications. In this work, catalysts with iron loadings of 1 wt%, 5 wt% and 10 wt% were synthesized by incipient wetness impregnation using water and acetone as solvents. The catalysts were calcined, reduced and tested in the selective acetylene hydrogenation under industrial front-end conditions. An activation behaviour of the catalysts due to the contact of the catalysts with air after the reduction is observed. After reaching a plateau in activity at 90 °C, the supported iron nanoparticles show excellent acetylene conversion of as well as excellent selectivities towards ethylene. No significant ethylene conversion was observed. This work demonstrates the great suitability of supported iron nanoparticles, especially for low iron loadings. The results show the need for further research in the development of iron-based catalysts. To increase the catalytic activity and enhance the reproducibility of the reduction process, the

development of a reactor concept with in situ reduction is important. This will shorten the activation phase and might lead to increased catalytic activity. Furthermore, the resilience of iron based catalysts against carbon monoxide in the reaction mixture must be tested and the effect on the activity and selectivity needs to be monitored. This is important to evaluate the suitability as industrial relevant catalyst. The development of iron-based bimetallic catalyst systems is of interest for the optimization of the catalytic activity and selectivity. Lastly, testing of different shaped α-alumina supports for improved flow behaviour should be part of further research and catalyst development.

Acknowledgment

The authors acknowledge financial support within the collaborative research center *'Iron upgraded!'* (CRC 1487) funded by the German Research Foundation (Grant No. 443703006).

Conflict of Interests

The authors declare no conflict of interest.

References:

[1] M. Takht Ravanchi, S. Sahebdelfar, S. Komeili, *Reviews in Chemical Engineering* **2018**, *34*, 215.
[2] A. Borodziński, G. C. Bond, *Catal. Rev. Sci. Eng.* **2008**, *50*, 379.
[3] A. Pachulski, R. Schödel, P. Claus, *Applied Catalysis A: General* **2012**, *445-446*, 107.
[4] S. Hock, L. Iser, M. Lucas, M. Rose, *Chemie Ingenieur Technik* **2022**, *94*, 1704.
[5] H. Zhou, X. Yang, L. Li, X. Liu, Y. Huang, X. Pan, A. Wang, J. Li, T. Zhang, *ACS Catal.* **2016**, *6*, 1054.
[6] M. Kuhn, M. Lucas, P. Claus, *Chem. Eng. Technol.* **2015**, *38*, 61.
[7] M. Kuhn, M. Lucas, P. Claus, *Ind. Eng. Chem. Res.* **2015**, *54*, 6683.
[8] A. Borodziński, G. C. Bond, *Cataly Rev* **2006**, *48*, 91.
[9] N. S. Schbib, M. A. García, C. E. Gígola, A. F. Errazu, *Ind. Eng. Chem. Res.* **1996**, *35*, 1496.
[10] M. R. Ball, K. R. Rivera-Dones, E. B. Gilcher, S. F. Ausman, C. W. Hullfish, E. A. Lebrón, J. A. Dumesic, *ACS Catal.* **2020**, *10*, 8567.
[11] I. Y. Ahn, J. H. Lee, S. S. Kum, S. H. Moon, *Catal. Today* **2007**, *123*, 151.
[12] M. Kuhn, M. Lucas, P. Claus, *Catal. Commun.* **2015**, *72*, 170.
[13] J. Gislason, W. Xia, H. Sellers, *J. Phys. Chem. A* **2002**, *106*, 767.
[14] A. J. McCue, J. A. Anderson, *Front. Chem. Sci. Eng.* **2015**, *9*, 142.
[15] S. Hock, C. V. Reichel, A.-M. Zieschang, B. Albert, M. Rose, *ACS Sustain. Chem. Eng.* **2021**, *9*, 16570.
[16] M. Tost, B. Bayer, M. Hitch, S. Lutter, P. Moser, S. Feiel, *Sustainability* **2018**, *10*, 2881.
[17] S. Meißner, *Resources* **2021**, *10*, 120.
[18] K. Islam, R. Yokoi, M. Motoshita, S. Murakami, *Resour. Conserv. Recycl.* **2022**, *183*, 106384.
[19] T. Norgate, S. Jahanshahi, *Miner. Eng.* **2011**, *24*, 1563.
[20] H. Zhou, X. Yang, A. Wang, S. Miao, X. Liu, X. Pan, Y. Su, L. Li, Y. Tan, T. Zhang, *Chinese J Catal* **2016**, *37*, 692.
[21] G. Vilé, D. Albani, M. Nachtegaal, Z. Chen, D. Dontsova, M. Antonietti, N. López, J. Pérez-Ramírez, *Angew. Chem. Int. Ed Engl.* **2015**, *54*, 11265.
[22] N. López, C. Vargas-Fuentes, *Chem. Commun. (Camb)* **2012**, *48*, 1379.

[23] D. Mei, M. Neurock, C. M. Smith, *J. Catal.* **2009**, *268*, 181.
[24] G. X. Pei, X. Y. Liu, A. Wang, A. F. Lee, M. A. Isaacs, L. Li, X. Pan, X. Yang, X. Wang, Z. Tai et al., *ACS Catal.* **2015**, *5*, 3717.
[25] B. Yang, R. Burch, C. Hardacre, P. Hu, P. Hughes, *Catal. Sci. Technol.* **2017**, *7*, 1508.
[26] P. A. Sheth, M. Neurock, C. M. Smith, *J. Phys. Chem. B* **2005**, *109*, 12449.
[27] G. X. Pei, X. Y. Liu, A. Wang, L. Li, Y. Huang, T. Zhang, J. W. Lee, B. W. L. Jang, C.-Y. Mou, *New J. Chem.* **2014**, *38*, 2043.
[28] J. Ballesteros-Soberanas, N. Martín, M. Bacic, E. Tiburcio, M. Mon, J. C. Hernández-Garrido, C. Marini, M. Boronat, J. Ferrando-Soria, D. Armentano et al., *Nat. Catal.* **2024**.
[29] Q. Feng, S. Zhao, Y. Wang, J. Dong, W. Chen, D. He, D. Wang, J. Yang, Y. Zhu, H. Zhu et al., *Journal of the American Chemical Society* **2017**, *139*, 7294.
[30] J. Osswald, K. Kovnir, M. Armbrüster, R. Giedigkeit, R. E. Jentoft, U. Wild, Y. Grin, R. Schlögl, *J. Catal.* **2008**, *258*, 219.
[31] J. Osswald, R. Giedigkeit, R. E. Jentoft, M. Armbrüster, F. Girgsdies, K. Kovnir, T. Ressler, Y. Grin, R. Schlögl, *J. Catal.* **2008**, *258*, 210.
[32] G. X. Pei, X. Y. Liu, X. Yang, L. Zhang, A. Wang, L. Li, H. Wang, X. Wang, T. Zhang, *ACS Catal.* **2017**, *7*, 1491.
[33] X. Cao, R. Tong, S. Tang, B. W.-L. Jang, A. Mirjalili, J. Li, X. Guo, J. Zhang, J. Hu, X. Meng, *Molecules* **2022**, *27*.
[34] S. Hock, M. Lucas, E. Kolle-Görgen, M. Mellin, J. P. Hofmann, M. Rose, *ChemCatChem* **2023**, *15*.
[35] X. Liu, Y. Li, J. W. Lee, C.-Y. Hong, C.-Y. Mou, B. W. Jang, *Applied Catalysis A: General* **2012**, *439-440*, 8.
[36] G. X. Pei, X. Y. Liu, A. Wang, Y. Su, L. Li, T. Zhang, *Applied Catalysis A: General* **2017**, *545*, 90.
[37] Y. Chen, J. Chen, *Appl. Surf. Sci.* **2016**, *387*, 16.
[38] B. Bridier, J. Pérez-Ramírez, *Journal of the American Chemical Society* **2010**, *132*, 4321.
[39] F. Studt, F. Abild-Pedersen, T. Bligaard, R. Z. Sørensen, C. H. Christensen, J. K. Nørskov, *Science* **2008**, *320*, 1320.
[40] B. J. Gregori, F. Schwarzhuber, S. Pöllath, J. Zweck, L. Fritsch, R. Schoch, M. Bauer, A. Jacobi von Wangelin, *ChemSusChem* **2019**, *12*, 3864.
[41] D. Faust Akl, A. Ruiz-Ferrando, E. Fako, R. Hauert, O. Safonova, S. Mitchell, N. López, J. Pérez-Ramírez, *ChemCatChem* **2021**, *13*, 3247.
[42] C. Rangheard, C. de Julián Fernández, P.-H. Phua, J. Hoorn, L. Lefort, J. G. de Vries, *Dalton Trans.* **2010**, *39*, 8464.
[43] M. Tejeda-Serrano, J. R. Cabrero-Antonino, V. Mainar-Ruiz, M. López-Haro, J. C. Hernández-Garrido, J. J. Calvino, A. Leyva-Pérez, A. Corma, *ACS Catal.* **2017**, *7*, 3721.
[44] B. Bridier, N. López, J. Pérez-Ramírez, *Dalton transactions (Cambridge, England : 2003)* **2010**, *39*, 8412.
[45] M. Tejeda-Serrano, M. Mon, B. Ross, F. Gonell, J. Ferrando-Soria, A. Corma, A. Leyva-Pérez, D. Armentano, E. Pardo, *Journal of the American Chemical Society* **2018**, *140*, 8827.
[46] J.-Y. Park, Y.-J. Lee, P. K. Khanna, K.-W. Jun, J. W. Bae, Y. H. Kim, *J. Mol. Catal. A Chem.* **2010**, *323*, 84.
[47] H.-J. Wan, B.-S. Wu, C.-H. Zhang, H.-W. Xiang, Y.-W. Li, B.-F. Xu, F. Yi, *Catal. Commun.* **2007**, *8*, 1538.

[48] M. Ates, V. Demir, Z. Arslan, J. Daniels, I. O. Farah, C. Bogatu, *Environ Toxicol* **2015**, *30*, 109.
[49] D. Mishra, R. Arora, S. Lahiri, S. S. Amritphale, N. Chandra, *Prot Met Phys Chem+* **2014**, *50*, 628.
[50] R. L. Frost, Y. Xi, H. He, *J. Colloid Interface Sci.* **2010**, *341*, 153.
[51] F. S. d. Santos, F. R. Lago, L. Yokoyama, F. V. Fonseca, *J. Mater. Res. Technol.* **2017**, *6*, 178.